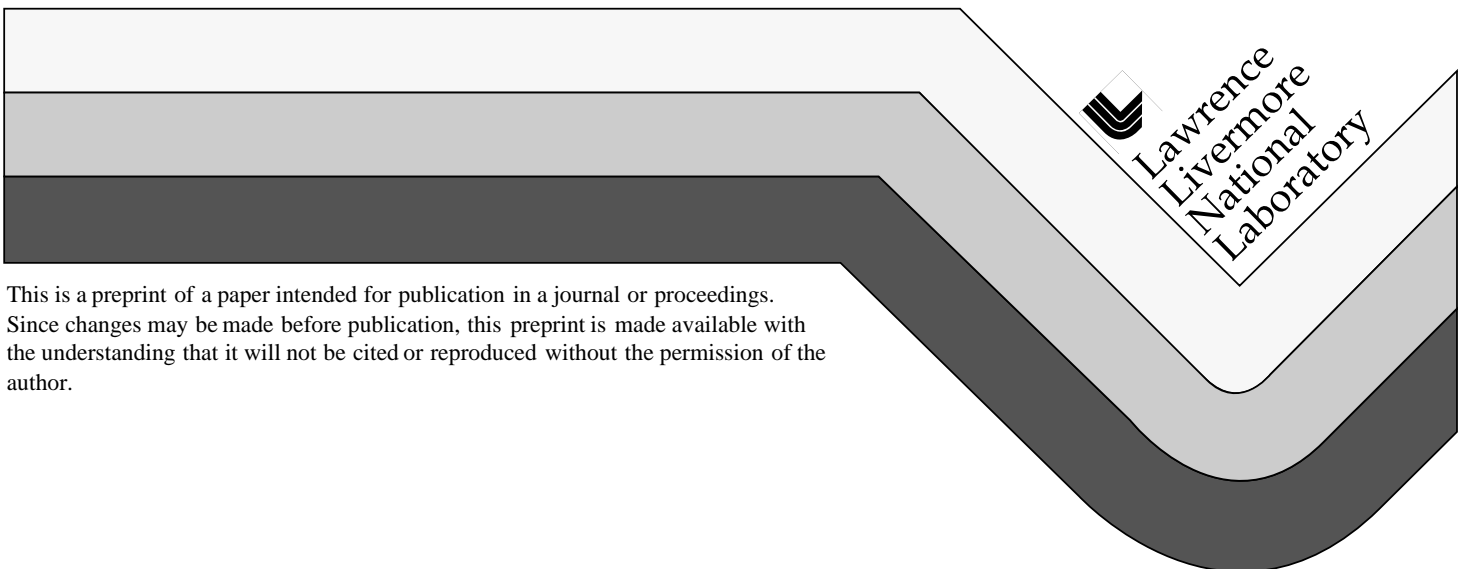


# High-Intensity-Laser-Driven Micro Neutron Sources for Fusion Materials Research at High Fluence

L. J. Perkins, B. G. Logan, M. D. Rosen, T. Diaz de la Rubia,  
N. M. Ghoniem, T. Ditmire, W. G. Wolfer

This paper was prepared for submittal to  
Nuclear Fusion

October 22, 1998



This is a preprint of a paper intended for publication in a journal or proceedings.  
Since changes may be made before publication, this preprint is made available with  
the understanding that it will not be cited or reproduced without the permission of the  
author.

#### DISCLAIMER

This document was prepared as an account of work sponsored by an agency of the United States Government. Neither the United States Government nor the University of California nor any of their employees, makes any warranty, express or implied, or assumes any legal liability or responsibility for the accuracy, completeness, or usefulness of any information, apparatus, product, or process disclosed, or represents that its use would not infringe privately owned rights. Reference herein to any specific commercial product, process, or service by trade name, trademark, manufacturer, or otherwise, does not necessarily constitute or imply its endorsement, recommendation, or favoring by the United States Government or the University of California. The views and opinions of authors expressed herein do not necessarily state or reflect those of the United States Government or the University of California, and shall not be used for advertising or product endorsement purposes.

# High-Intensity-Laser-Driven Micro Neutron Sources for Fusion Materials Applications at High Fluence

L. J. Perkins, B. G. Logan, M. D. Rosen, M. D. Perry, T. Diaz de la Rubia,  
N. M. Ghoniem\*, T. Ditmire, W. G. Wolfer

*Lawrence Livermore National Laboratory*  
September 14, 1998

## Synopsis

We investigate the application of fast pulse, high intensity lasers to drive low cost, deuterium-tritium (DT) neutron sources for fusion materials testing at high flux/fluence. Today, high power bench-top lasers with intensities of  $10^{18}\text{W}/\text{cm}^2$  are routinely employed and systems capable of  $\geq 10^{21}\text{W}/\text{cm}^2$  are becoming available. These potentially offer sufficient energy density for efficient neutron production in DT targets with dimensions of around  $100\mu\text{m}$ . We study two different target concepts – a hot ion, beam-target system and an exploding-pusher target system – and evaluate neutron production as a function of laser and target conditions. Compared with conventional beam-target neutron sources, the small source volume and heat removal by sacrificial vaporization can yield high fluxes of  $14\text{MeV}$  neutrons at close-coupled, micro-test specimens of characteristic dimensions  $\sim 0.1\text{--}1\text{mm}$ . In particular, we show that a laser-driven target with  $\sim 100\text{J}/\text{pulse}$  at  $100\text{Hz}$  and laser irradiances in the range  $I\lambda^2 \sim 10^{17}\text{--}10^{19}\text{W}\cdot\mu\text{m}^2/\text{cm}^2$  could produce primary, uncollided neutron fluxes at the test specimens in the range  $10^{14}\text{--}10^{15}\text{ n}\cdot\text{cm}^{-2}\cdot\text{s}^{-2}$ . By adjusting the laser pulse repetition rate from below  $10\text{Hz}$  to above  $50\text{Hz}$ , such a facility could be tailored to yield information on both the pulsed damage and steady-state damage sustained by inertial and magnetic fusion systems, respectively. We then describe the complementary materials science and computational modeling research required to validate damage models for  $\geq 100\text{dpa}$  irradiation of such specimens and to provide a multiscale predictive capability for the behavior of engineering-scale components in fusion reactor applications. Principle issues requiring further R&D include: (a) Quantitative experimental data on the interaction of fast-pulse, high intensity lasers with targets, particularly the mechanisms for high efficiency fast ion production; (b) Experiments with candidate targets to project neutron yields and fusion gains attainable with affordable laser energies of  $\sim 100\text{J}$  to  $1\text{kJ}$ , repetition rates of  $\sim 10\text{--}100\text{Hz}$ , and average power levels of  $\leq 10\text{kW}$ ; (c) Engineering designs of practical laser-target systems for the standoff and protection of close-coupled micro-materials specimens; (d) A materials science/computational effort to couple specimen evaluations to multi-scale, predictive modeling codes.

---

\* University of California, Los Angeles

## 1. Rationale and Overview

The irradiation environment of DT fusion reactors, both inertial and magnetic, consists of 14.1MeV neutrons plus a large fraction (~80% at the first wall surface) of lower energy, collided neutrons. For a neutron wall load, i.e., neutron power flux, at the first wall of, say,  $5\text{MWm}^{-2}$ , the primary, uncollided inward flux is  $2.2 \times 10^{14} \text{ n.cm}^{-2} \text{ s}^{-1}$  and the total flux is in excess of  $10^{15} \text{ n.cm}^{-2} \text{ s}^{-1}$ . In magnetic fusion reactors with solid walls and inertial fusion reactors with thin, wetted walls guided by solid or compliant structures, significant damage will be sustained. A number of specific reactions result from such neutron interactions including tritium and helium production, atomic displacements and transmutations [1]. Detrimental consequences include changes in thermophysical and thermomechanical properties, swelling, embrittlement, creep and sintering. End-of-life damage limits are estimated to be around 100–200 displacements-per-atom (dpa) for metals and in the range 10–50 dpa for non-metals such as ceramics and composites [1, 2]. These correspond to primary neutron fluences, i.e., time-integrated fluxes, of approximately 10–20 MW-yr/m<sup>2</sup> ( $\approx 1.4\text{--}2.8 \times 10^{22} \text{ n.cm}^{-2}$ ) and 1–5 MW-yr/m<sup>2</sup> ( $\approx 1.4\text{--}7 \times 10^{21} \text{ n.cm}^{-2}$ ), respectively. Thus damage due to neutrons is a crucial factor in determining design limits and predicted lifetimes for fusion structural and blanket materials. Of course, the cost of obtaining such materials damage data is an important issue, especially where DT neutrons are concerned. Minimizing the source volume is one way to reduce cost through significantly lower drive requirements and tritium inventories.

Point neutron sources offer an attractive option for materials irradiation testing because of their simplicity, easy access and relatively low cost. From the descriptions above, the desired characteristics of such sources are:

- Capability of producing high damage rates in the range 20–100 dpa/year corresponding to primary, uncollided neutron fluxes of  $\sim 1\text{--}4 \times 10^{14} \text{ n.cm}^{-2} \text{ s}^{-1}$  (i.e.,  $\sim 2\text{--}10 \text{ MWm}^{-2}$  for DT neutrons)
- Small neutron source volume for low cost. A test specimen cannot be placed closer than a distance determined by the emitting volume plus the heat removal hardware.
- A neutron source energy which provides a damage spectrum similar to that of a DT fusion reactor;  $\Rightarrow$  a 14MeV DT neutron source is highly desirable
- High availability over extended periods of time

The last ten years or so has witnessed an explosion in the field of short-pulse, high-intensity lasers research and development [3, 4]. Pulse lengths have reduced from tens of picoseconds in the mid-1980's to state-of-the-art ~10 femtoseconds today. Second, the ability to generate light pulses three orders of magnitude shorter means that, for the same energy and same approximate cost, intensities have increased by the same factor. Thus today intensities of  $10^{18}$  W/cm<sup>2</sup> are routinely available from table-top lasers and systems capable of  $\sim 10^{21}$  W/cm<sup>2</sup> are now starting to come on line. In particular, access to high temperature states of matter capable of thermonuclear fusion and/or the efficient production of hot ions for beam-target fusion is now within reach using small-scale, bench-top lasers.

Accordingly, in this paper, we investigate the prospects for utilizing such intense, bench-top-scale laser systems to drive low-cost, intense 14MeV DT neutron sources in either fast-ion-driven micro-targets or exploding pushers. Such targets permit the close coupling of small ( $\leq 0.1$ –1mm) micro test specimens of metals, carbon, silicon carbide, etc. and the potential of obtaining neutron fluxes in the  $10^{14}$ – $10^{15}$  n.cm<sup>-2</sup>s<sup>-1</sup> range. A complementary materials science and computational modeling program described below would validate damage models for  $\geq 100$ dpa materials lifetime and provide a multiscale predictive capability for the extrapolated behavior of, engineering-scale components. Such a coupled irradiation-computation program could partially compensate for the absence of large scale testing with high-fluence, volumetric fusion plasmas.

In the following, we describe three candidate target concepts for high yield laser-driven neutron sources. Concepts 1 and 3 will be considered in further detail below:

### *(1) Thin target, fast-ion, beam-target source*

A thin ( $\sim 1\lambda$ ), isolated laser 'foil' target of frozen tritium is suspended above a thicker substrate layer of deuterium. Laser energy absorbed by hot electrons electrostatically couple to ions in the foil resulting in the efficient production of fast tritium ions in the ~100's keV range. The inward-directed tritons undergo beam-target fusion reactions with the deuterium in the substrate. Fast ion heating raises the latter's electron temperature in the range of 100's eV–keV, thus reducing the ion stopping power for subsequent ions and significantly enhancing the neutron production rate per laser energy pulse. As discussed below, this scheme is applicable to laser irradiances in the approximate range  $I\lambda^2 \sim 10^{16}$ – $10^{18}$  W- $\mu\text{m}^2/\text{cm}^2$ , otherwise the fast ions are too slow or too energetic, respectively. The majority of analysis in this paper will be devoted to this type of target.

## *(2) Thick target, high-intensity-driven, beam-target source*

At higher laser irradiances  $I\lambda^2 \geq 10^{18} \text{ W}\cdot\mu\text{m}^2/\text{cm}^2$ , plasma electrons can be driven relativistically. Hole-boring of the laser light yields electron-driven acceleration gradients producing energetic ions. At very high irradiances  $\geq 10^{20} \text{ W}\cdot\mu\text{m}^2/\text{cm}^2$ , efficient energy transfer to fast ions can occur by collisionless shock heating. Here, direct momentum transfer from the laser light to the ions drive the latter into the target. Unlike the analogous scheme in (1) above, this produces fast ions directly for beam-target fusion without the need for the thin target layer isolated from the substrate. In this case, a single, thick cryogenic target layer of 50:50 DT might be employed of thickness equal to the optimum ion range, thus considerably simplifying target fabrication but at the expense of higher laser intensities in the range  $10^{18}$ – $10^{20} \text{ W}\cdot\mu\text{m}^2/\text{cm}^2$  and higher tritium inventories. Other considerations of the beam-target neutron production will be similar to those discussed below in connection with the analysis for Concept-1.

## *(3) Exploding-pusher-target source*

Hot electrons from a high-intensity laser strike the outside of a thin ( $\sim$ few  $\mu\text{m}$ ) metal or glass shell enclosing a cryogenic solid or liquid DT core. The shell heats rapidly to  $\sim$ keV temperatures, exploding the shell with many gigabar pressures and driving an inward shock at  $\sim$ several  $\times 10^7 \text{ cm/s}$ . The convergent shock heats the DT core yielding ion temperatures in the  $\geq 10 \text{ keV}$  range. Fuel burnup and resulting neutron yield is determined by the dynamics of capsule disassembly

We also note that irradiation of noble-gas clusters ( $\sim 1000$ 's atoms/cluster) with high-intensity laser pulses have produced highly ionized, very high temperature micro-plasmas [5, 6]. The explosion of these micro-clusters ejects ions with high kinetic energy. Beam-target neutrons could be produced from such fast ions in a manner analogous to the thin-target, hot-ion concept in Concept-1 above but with rather different target geometries. In particular, Ditmire has shown that in such clusters, the efficiency of absorption of laser energy into fast ions can be in excess of 80% for laser intensities of  $\sim 10^{16} \text{ W/cm}^2$  [6]. The mean fast ion energy here was  $\sim 45 \text{ keV}$ . Although the mechanism for such efficient hot ion production is not clear, it may be that the clusters are acting similar to thin foils where space-charged limiting electrons accelerate ions from the resulting potential sheath.

Fig. 1 shows a schematic view of a neutron facility based on Concepts 1 through 3 above. The system is driven by a high intensity, rep-rateable laser of  $\sim 100$ – $1000 \text{ J/pulse}$ , at  $\sim 10$ – $100 \text{ Hz}$  ( $\sim 10 \text{ kW}$  average power), with pulse duration and focal spot sent by the irradiance ( $I\lambda^2$ ) requirements of the neutron-

producing target (see below). The targets of a few 10's of  $\mu\text{m}$  diameter are mounted  $\sim 1\text{-}10\text{cm}$  apart on a continuous foil strip which moves each target into the firing position at speeds of  $\sim 0.1\text{-}10\text{m/s}$ . A sacrificial foil debris shield moving with the targets protects the material specimen matrix which is coupled as closely as running clearances permit (typically  $\leq 0.2\text{cm}$  from the front face of the specimen to the center of the neutron production volume). We will examine the target and neutron source geometries for Concepts 1 and 3 in further detail below.

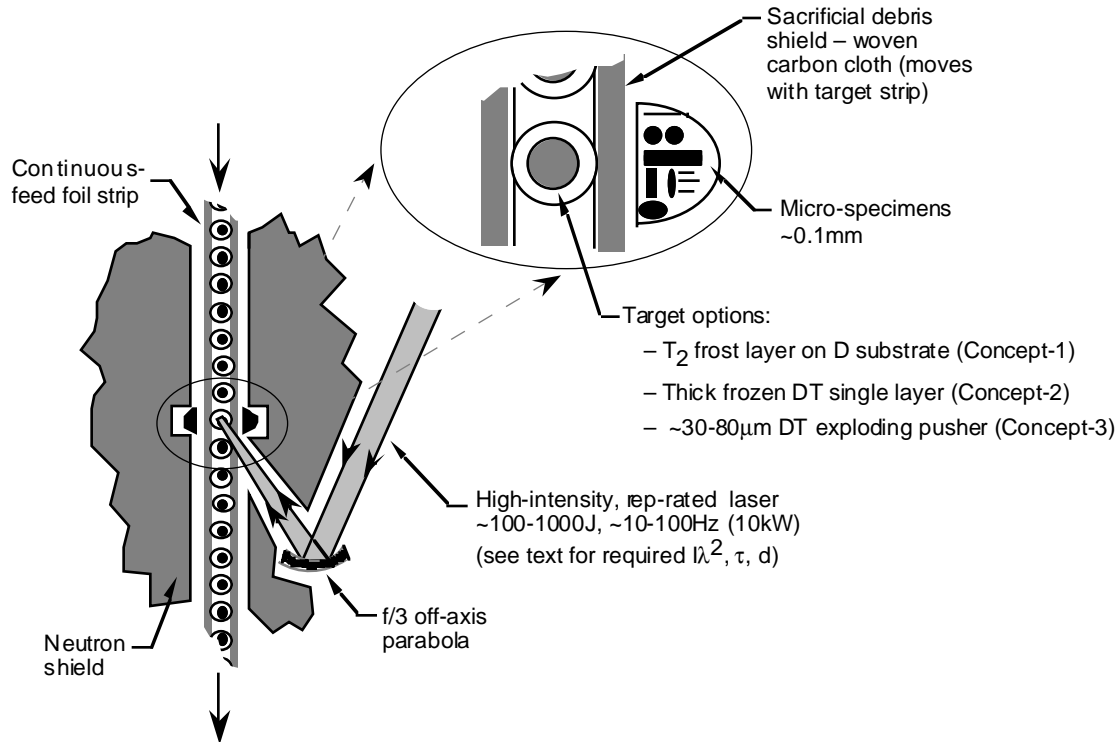


Fig.1. Schematic view of the micro-DT neutron source driven by a short pulse, high average power laser (not to scale). Target concepts 1 –3 are described in the text and the target design for Concept-1 is shown in Fig. 2 below

A possible alternative to the continuous target strip is to inject the targets in a manner similar to that envisaged for inertial confinement fusion reactors [7]. This might be particularly applicable to the exploding pusher targets of Concept-3. However, this injection option would need careful attention to minimize target-specimen standoff distances otherwise neutron fluxes at the specimen will be significantly reduced.

In Table 1, we compare the main features of these laser-driven schemes with other candidate neutron sources for fusion materials testing. Some, like the subject of this paper are in the conceptual stage while others have seen considerable prior use.

Table 1. Classes of neutron sources for fusion material testing

	Description	Examples*	Neutronics Specifications	Dimensions of Emitting Volume	Input Power — Facility Cost — Tritium Usage	Comments
<b>Laser-Based, Micro Neutron Sources</b>	High-intensity, laser-driven; close-coupled, micro samples	• Hot-ion beam-target • Exploding pusher target (c)	$\sim 10^{14}$ - $10^{15}$ $\text{cm}^{-2}\text{s}^{-1}$ over micro samples (100 $\mu\text{m}$ -1mm). 14MeV DT spectrum	$\sim 0.05\text{cm}$ (fast ion range in substrate)	$\sim 10\text{kW}$ . <\$200M. $\sim 3 \times 10^{-4}$ g/day	This paper. Low cost. High fluxes. Small testing volume ( $\sim 0.5\text{cm}^3$ ), specimen sizes of $\sim 0.1$ -1mm.
<b>Accelerator-Based, D-T Beam-Target</b>	$\sim 370\text{keV}$ , $\sim 150\text{mA}$ deuterium beam; H <sub>2</sub> O-cooled T-Zr target	• RTNS-II (s)	$\sim 5 \times 10^{12}$ $\text{cm}^{-2}\text{s}^{-1}$ over 1 $\text{cm}^3$ test volume. 14MeV DT spectrum	$\sim 1\text{cm}$ (beam spot diameter)	$\sim 50\text{kW}$ . $\sim \$25\text{M}$ . $\sim 2 \times 10^{-5}$ g/day	Heat removal at large, water-cooled solid target limits flux and fluence. Not relevant for high flux/fluence
<b>Accelerator-Based, D-Li Beam-Target</b>	$\sim 30$ -40MeV, $\sim 250\text{mA}$ deuterium beam on liquid lithium target.	• IFMIF (c)	$\sim 9 \times 10^{13}$ ( $2.2 \times 10^{14}$ ) $\text{cm}^{-2}\text{s}^{-1}$ over 500 (100) $\text{cm}^3$ test volumes. D-Li neutron spectrum	$\sim 10\text{cm}$ (beam footprint)	$\sim 10\text{MW}$ . $\sim \$1\text{B}$ . N/A	Neutrons from forward-peaked, stripping reaction. Most efficient beam-target neutron producing reaction. Uncertainties in damage relevance due to $E_n \geq 20$ -40MeV
<b>Spallation Sources</b>	800MeV-GeV's proton beam at $\sim 10$ 's mA on water-cooled tungsten	• LANSCE (o) • IPNS (c)	$\leq 10^{13}$ $\text{cm}^{-2}\text{s}^{-1}$ over $\sim 20 \times 10^3$ $\text{cm}^3$ test volumes. Spallation neutron spectrum	$\sim 10$ 's cm to m's (proton range)	$\sim 10$ 's MW. $\sim \$\text{B}'\text{s}$ for new facilities N/A	Significant uncertainties in damage relevance due to spallation spectral components ( $E_n \gg 20\text{MeV}$ )
<b>Fusion-Based High-Flux Sources</b>	Neutral-beam-heated 200eV mirror plasma. 0.17-1.1 MW fusion power	• BPNS (c) • GDT (c)	$\geq 4(1) \times 10^{14}$ $\text{cm}^{-2}\text{s}^{-1}$ over 600 $\text{cm}^3$ ; $\geq 10^{13}$ over 0.6 (0.04) $\text{m}^3$ . 14MeV DT spectrum	$\sim 20(10)$ cm (neutral beam range in target plasma)	60(13) MW. $\sim \$1(0.5)\text{B}$ . $\sim 0.9\text{g/day}$	Most fusion-relevant. Medium test volumes. Probably dependent on international fusion development strategy.
<b>Fusion-Reactor Volumetric Sources</b>	High average-power MFE or IFE test facilities. Typically driven at moderate Q	• VNS (mfe) (c) • ETF (ife) (c)	$\sim 4 \times 10^{13}$ - $2 \times 10^{14}$ $\text{cm}^{-2}\text{s}^{-1}$ . Large volumes ( $\sim \text{m}^3$ ). 14MeV DT spectrum	$\sim 2\text{m}$ (plasma minor diameter)	$\sim 100$ 's MW. $\sim \$3$ -5B. $\sim 8\text{g/day}$	Most fusion-relevant. Large test volumes. Significant cost. Probably dependent on international fusion development strategy
<b>Fission Reactors</b>	In-core specimens in existing fission reactors	• HFIR (o) • HFBR (o/s) • ATR (o)	$10^{14}$ - $2 \times 10^{15}$ $\text{cm}^{-2}\text{s}^{-1}$ , 10's $\text{cm}^3$ volumes. Fission neutron spectrum	$\sim 1\text{m}$ (core diameter)	$\sim 100$ 's MW $\sim \$\text{B}'\text{s}$ for new facilities N/A	Thermal or mixed fission spectrum; not very fusion relevant. High flux. Available facilities will decline in future years

\* (o) = operating. (s) = shut down. (c) = conceptual design. RTNS-II = Rotating Target Neutron Source (LLNL); IFMIF = Internat. Fusion Materials Irradiation Facility; BPNS = Beam Plasma Neutron Source; GDT = Gas-Dynamic Trap; VNS = Volumetric Neutron Source (spherical tokamak); ETF = IFE Engineering Test Facility; HFIR = High Flux Irradiation Reactor (ORNL); ATR = Advanced Test Reactor (Naval, INEL); HFBR = High Flux Beam Reactor (BNL); SNS = Intense Pulsed Neutron Source (ORNL); LANSCE = Los Alamos Neutron Science Center

Fission reactors are presently the workhorse for high flux testing of fusion materials. Unfortunately, conditions in a fission reactor are not the same as those expected in a fusion reactor. Neutron energy spectra are different, with the consequence that the generated recoil spectrum in materials is different [2]. Moreover, large quantities of helium and transmutation products will be produced in threshold (n,X) reactions in the fusion environment which are not present in fission reactors. We note also from Table 1 the possibility of employing existing or near-term spallation neutron sources. However, it has been judged that spurious charged particle production due to the high energy tail of the neutron spectrum ( $\gg 20\text{MeV}$ ) and the low dpa generation rate make these of limited use to fusion materials research [8].

In the absence of a test facility with a prototypical fusion spectrum, fission reactors will continue to remain the primary facilities for fusion materials irradiation. The value of fission reactors can be enhanced by innovative techniques to better simulate helium and hydrogen production through, for example, helium charging and boron or nickel doping. However, in a fusion reactor, the projected helium-to-dpa ratio is typically  $\sim 4\text{-}15$  appm/dpa for vanadium alloys and ferritic steels, and an order of magnitude higher in SiC and graphite. Deeper in the structure where the neutron spectrum is softer, these ratios drop because of their typically higher energy thresholds and fission simulations become more relevant. But in the critical first few neutron-mean-free-paths from the first wall, the primary damage state for microstructural and compositional changes is rather dissimilar for fission and fusion irradiation. An example is the helium-production reactions in carbon-bearing materials where the  $^{12}\text{C}(n,\alpha)$  and  $^{12}\text{C}(n,3\alpha)$  reactions have thresholds of 6.2MeV and 8.3MeV, respectively.

Hence, no existing neutron source offers the necessary combination of neutron flux, spectrum and cost-effectiveness. Relative to the other candidates in Table 1 and, in particular, to the other beam-target sources, the laser-driven concepts of this paper may offer the following advantages:

- Very small target volumes due to very high laser intensities and heat removal by sacrificial vaporization rather than by the steady-state, liquid cooling methods of conventional beam-target neutron sources [see, for example, Refs. 9, 10]. This provides the opportunity to close-couple irradiation specimens resulting in very high point neutron fluxes at low power and low cost.
- The prospects for self-heated plasma targets. In the case of the fast ion beam-target schemes in Concepts-1 and 2, this provides significantly higher neutron production rates per incident Watt relative to conventional, beam-target neutron sources with cold targets.

- Low cost. The cost of fast-pulse, intense lasers scale approximately as the energy per pulse with pulse length and rep-rate only a secondary cost issue up to some heat-removal limit. Thus, the average power of the system and, therefore, the time-averaged neutron flux is ultimately determined by the heat removal limitations in the laser.
- The production of a pure DT neutron spectrum. This provides for material irradiation experiments that are free of the spectral uncertainties accompanying irradiations in fission reactors, spallation sources and D-Li beam-target systems.

Of course, the small source volumes and close-coupling means that the useful testing volume in the high flux zone is only of the order of  $0.5\text{cm}^3$ . However, as discussed below, we believe that the small dimensions of the specimens envisaged for use here ( $\sim 0.1\text{-}1\text{mm}$ ) do not present any fundamental difficulty regarding experimental characterization of the irradiated volumes.

## 2. Laser Interaction Physics And Requirements for Neutron Production.

A review of the literature on high intensity lasers from the past decade or so indicates that it is convenient to separate the laser interaction physics for our neutron sources into three different irradiance regimes:

### 1. $I\lambda^2 < 10^{17}\text{W}\cdot\mu\text{m}^2/\text{cm}^2$

At lower intensities,  $I\lambda^2 < 10^{17}\text{W}\cdot\mu\text{m}^2/\text{cm}^2$ , the interaction of laser light takes by inverse Bremsstrahlung and collisional absorption [11]. For the target of Concept-1 operating in this regime, laser energy is initially absorbed entirely by plasma electrons. However, in the thin, isolated target layer, the space charge field of the heated electrons accelerates ions into the blow-off plasma and the frost layer explodes [see, for example, Ref. 12], resulting in significant fast ion production. In thicker, single-region targets at these lower intensities, we would expect that electron heat conduction into the target coupled with the neutralizing effect of the cold returning electron current would result in little hot ion production.

From a review of experiments in the range  $I\lambda^2 \sim 10^{11}\text{-}10^{17}\text{W}\cdot\mu\text{m}^2/\text{cm}^2$ , Gitomer [13] suggests a hot electron scaling of the form:

$$T_{e,hot}(keV) \sim 1.6 \times 10^{-6} [I\lambda^2 (\text{W}\mu\text{m}^2 / \text{cm}^2)]^{4/9} \quad (1)$$

He applies three analytic models to deduce the mean fast ion energy as

$$\bar{E} \text{ (keV / amu)} \sim k_1 \cdot T_{e,hot} \text{ (keV)} \quad (2)$$

with  $k_1$  from the models being in the range  $2/3^{1/2}$  to 12.5. Experimental data in the range  $I\lambda^2 \leq 10^{17} \text{W-}\mu^2/\text{cm}^2$  appear to be well fit by  $k_1 \sim 4-5$ .

This scaling for fast ion energy is in agreement with the fact that the ion rich plasma resulting from expelled electrons should exhibit a sheath potential of [14]

$$V_{sheath} \sim \frac{kT_{e,hot}}{2e} \ln \left[ \frac{m_i}{2\pi m_e} \right] \quad (3)$$

Similar scalings from Kruer and Estabrook, and Kruer [15] suggest

$$T_{e,hot} \text{ (keV)} \sim k_2 [I\lambda^2 (\text{W}\mu^2 / \text{cm}^2)]^{0.33} \quad (4)$$

where  $k_2$  is in the range  $6 \times 10^{-5}$  to  $1.2 \times 10^{-4}$ .

Fews et al [16] have presented recent experimental evidence for such ion energies of  $\sim 0.2$  to  $1.3 \text{MeV}$  for intensities of  $I = 2 \times 10^{17} - 2 \times 10^{18} \text{W/cm}^2$ . Also, as noted above, Ditmire has measured the absorption efficiency of laser energy into fast ions with peak laser intensities of  $2 \times 10^{16} \text{W/cm}^2$  incident on clusters ( $\sim 1000$ 's atoms/cluster) [5, 6]. He finds mean fast ion energies of  $\sim 45 \text{keV}$  and absorption efficiencies of 80-90%. Presumably the superheated clusters act like a collection of individual, space-charge-limited thin targets.

## 2. $I\lambda^2 \sim 10^{18} \text{W-}\mu^2/\text{cm}^2$

Collisional absorption becomes ineffective at irradiances of  $I\lambda^2 \geq 10^{17} \text{W-}\mu^2/\text{cm}^2$  because the plasma temperature rises too quickly for collisions to be effective (note that the electron-ion collision frequency goes as  $\nu_{ei} \sim n/T_e^{3/2}$ ) In addition, at  $10^{18} \text{W-}\mu^2/\text{cm}^2$  the electron quiver velocity becomes comparable to the thermal velocity. In particular, the electron quiver energy  $E_{osc}$ , (i.e., the cycle-averaged, oscillatory energy of the electron in the laser field) is  $\sim 100 \text{keV}$  at  $10^{18} \text{W-}\mu^2/\text{cm}^2$  [3] requiring a relativistic treatment of the interaction process. This can result in relativistic self-focusing and channel formation leading to laser 'hole boring'. The hot electron energy can be several times  $E_{osc}$  and fast ions can then be accelerated through this  $\sim \text{MeV}$  electron-induced channel.

The hot electron temperature also depends on the polarization of the laser field, with p-polarization – that is, polarized in the plane of propagation – exhibiting 2-3 times the hot electron temperature over s-polarization at the same laser intensity [17, 18]. Wilkes et al [17] have performed PIC simulations at irradiances of  $10^{18}$ – $10^{19}$ W- $\mu\text{m}^2/\text{cm}^2$ . At  $10^{19}$ W- $\mu\text{m}^2/\text{cm}^2$  they determined  $T_e \sim 1.4\text{MeV}$  for p-polarized light and also find fast ion energies of  $\sim 10^{-3}m_0c^2$  at the same intensity which translates to  $\sim 2\text{MeV}$  for deuterons. Guethlein [19] has measured hot ion energies in excess of 1MeV for laser intensities of  $2$ – $3 \times 10^{19}$ W/cm<sup>2</sup> incident on aluminum and plastic targets.

Pretzler et al [20] have observed DD neutron production through this proposed mechanism in deuterated polythene, using a 160fs, 200mJ laser with a  $4.5\mu\text{m}$  focal spot ( $\Rightarrow I \sim 10^{18}$ W/cm<sup>2</sup>). Two effects are suggested to contribute to the channel formation. First, the relativistic mass increase of the quiver electrons in the focal region causes an increase in the refractive index and forms an effective positive lens. Second, as the sub-MeV electrons are accelerated forward, they generate megagauss fields leading to self-pinching of both the electrons and the light. Note that in any event, the light pressure itself exceeds the plasma pressure. The result is a single, narrow light propagation channel with diameter of several wavelengths and elongated over many Rayleigh lengths — i.e., the length for 1/e diffraction expansion. Not surprisingly, this regime is not well modeled by classical Spitzer-Harm conductivity.

Norres et al [21] have observed similar beam-target DD neutron production with 1.3ps,  $1.05\mu\text{m}$  light on flat targets of  $120\mu\text{m}$ -thick deuterated polystyrene ( $\text{C}_8\text{D}_8$ ) and also cryogenic deuterium pellets 0.5cm thick. They ran with  $\sim 8$ – $20\text{J}$  and average intensities of  $\sim 8 \times 10^{18}$ W/cm<sup>2</sup>. Their quoted DD yields of  $7 \times 10^7$ neutrons/sr would result in a fusion Q-value (= fusion energy divided by laser input energy) of  $\sim 2\%$  if operated in DT. As shown below, this implies both an efficient transfer of laser energy into fast ion energy and beam-target interactions within a high temperature plasma background

### 3. $I\lambda^2 \geq 10^{20}\text{W}\text{-}\mu\text{m}^2/\text{cm}^2$

At these very high intensities, the light pressure,  $P = 2I/c \sim 600 \times I(\text{W}/\text{cm}^2)/10^{18}$  Mbar, vastly exceeds the plasma pressure and momentum conversion from the ponderomotive force of the laser can occur directly to fast ions with high efficiency. Under such conditions, the properties of the plasma so produced are determined by the laser field rather than by its hydrodynamics. Note that, at  $I = 10^{20}$ W/cm<sup>2</sup>, the light pressure is  $\sim 6 \times 10^4$  Mbar. The resulting collisionless shock can compress ion densities to several times that of the original pre-formed plasma [22]. Also, there are

significant differences in the electron interaction physics relative to that occurring at lower intensities. First, because of the very short pulse duration, there is insufficient time for a substantial region of coronal plasma to form in front of the target. That is, the hydrodynamic time scale is longer than the pulse length. Second, because of the steep density gradients and hole boring, the laser energy is deposited at much higher electron densities than the critical density which would otherwise limit long pulse penetration.

In this high intensity limit, momentum conservation yields ion velocities of

$$V_{ion} = 2 (I/\rho c)^{1/2} \quad (5)$$

implying that the mean fast ion energy should scale as  $\sim I$  rather than the  $\sim I^{-0.3-0.5}$  at lower intensities. Thus at  $10^{20}\text{W}/\text{cm}^2$  in a deuterium target, this direct process should yield deuterons with energies approaching an MeV or so.

Denavit [22] has performed PIC simulations of interactions at  $I = 10^{20}$ – $10^{21}\text{W}/\text{cm}^2$  in thin, solid targets, demonstrating light transmission through plasmas which are overdense by factors of  $10^2$ – $10^3$ . Similarly, Lawson et al [23] have modeled intensities in the range  $I = 10^{18}$ – $10^{22}\text{W}/\text{cm}^2$  in thin foils of aluminum and CH plastic. They find ions in the range of several hundred keV at  $I=10^{20}\text{W}/\text{cm}^2$  consistent with Eq. 5 above and  $\sim 25\%$  energy absorption efficiency into ions at  $I=10^{21}\text{W}/\text{cm}^2$ . Note however that both Denavit and Lawson et al.'s results apply to thin targets  $\ll 1\lambda$  which presumably will be influenced by electron space charge production.

### *Implications for Efficient Neutron Production*

From the evidence above, it appears that fast ion energies around 100-1000keV are attainable in thin targets for laser irradiances of  $\leq 10^{17}\text{W}\cdot\mu\text{m}^2/\text{cm}^2$  due to acceleration by the space-charge-limited electron field and, interestingly, energies of the same order may be attainable for  $I\lambda^2 \sim 10^{18}$  to  $>10^{20}\text{W}\cdot\mu\text{m}^2/\text{cm}^2$  in thick targets due to relativistic hole boring and/or direct momentum transfer from the laser field. Moreover, energy conversion efficiencies into ions of  $\sim$  tens of % may be available throughout this range [6-7, 13, 17, 22-24]. In general, scaling of hot ion energies and efficiencies tend as  $I^x$  where  $x\sim 0.3-0.5$  in the lower intensity regime and  $x\sim 1$  in the high intensity regime.

To date there is no single model which can accommodate all the features of the interaction physics. Nor can present models adequately describe the transitions from lower to higher intensities, especially the effects

of relativistic hole boring, the electron transport in resulting high magnetic fields which persist on the hydro time scale, and the resulting energy coupling to ions. This situation calls for quantitative experiments. In particular, experiments are needed to determine the laser conditions at high intensity that would allow us to dispense with the thin, multilayer target geometry of Concept-1 above and employ the simpler single, thick target idea of Concept-2.

Thus, in the case of these beam-target schemes, an efficient, high-Q neutron source will require attention to the following:

- Efficient coupling of laser energy to hot electrons in the target
- Efficient coupling of electron energy into fast ions or, at very high intensities, the efficient production of fast ions directly by the laser field.
- The production of fast ions in the energy range of several hundred keV to optimize DT neutron yield per unit laser energy dissipated in the target. Higher ion energies in the MeV range result in lower fusion Q values and have long range in the target substrate thus increasing the target-sample standoff distance (see below).
- Concurrent heating of the target substrate to  $\geq 100\text{eV}$  to decrease the fast ion atomic stopping power and enhance the neutron yield per unit energy deposited in the target

### **3. Thin Target, Hot Ion, Beam-Target Neutron Source (Concept-1).**

Fig 2. shows a schematic target design for Concept-1. A thin ( $<1\lambda$ ) layer of tritium frost is suspended above a frozen deuterium substrate of thickness 10's–100's  $\mu\text{m}$  depending on the fast ion energy and substrate electron temperature. Laser energy is absorbed by electrons in the tritium layer which become space-charged limited as they stream from the interaction region. Their energy is electrostatically coupled into ions and fast tritons are pulled explosively out of the target layer and enter the deuterium substrate. Depending on laser and target conditions an appreciable fraction of the incident laser energy can be converted to hot ions with energies in the range 100's keV to  $\sim 1$  MeV. The re-entrant conical target assembly is employed to enhance the inward-direct ion current. Alternatively, we could consider a substrate of either a low density foam filled with cryogenic  $\text{D}_2$  or a frozen  $\text{CD}_4$  layer.

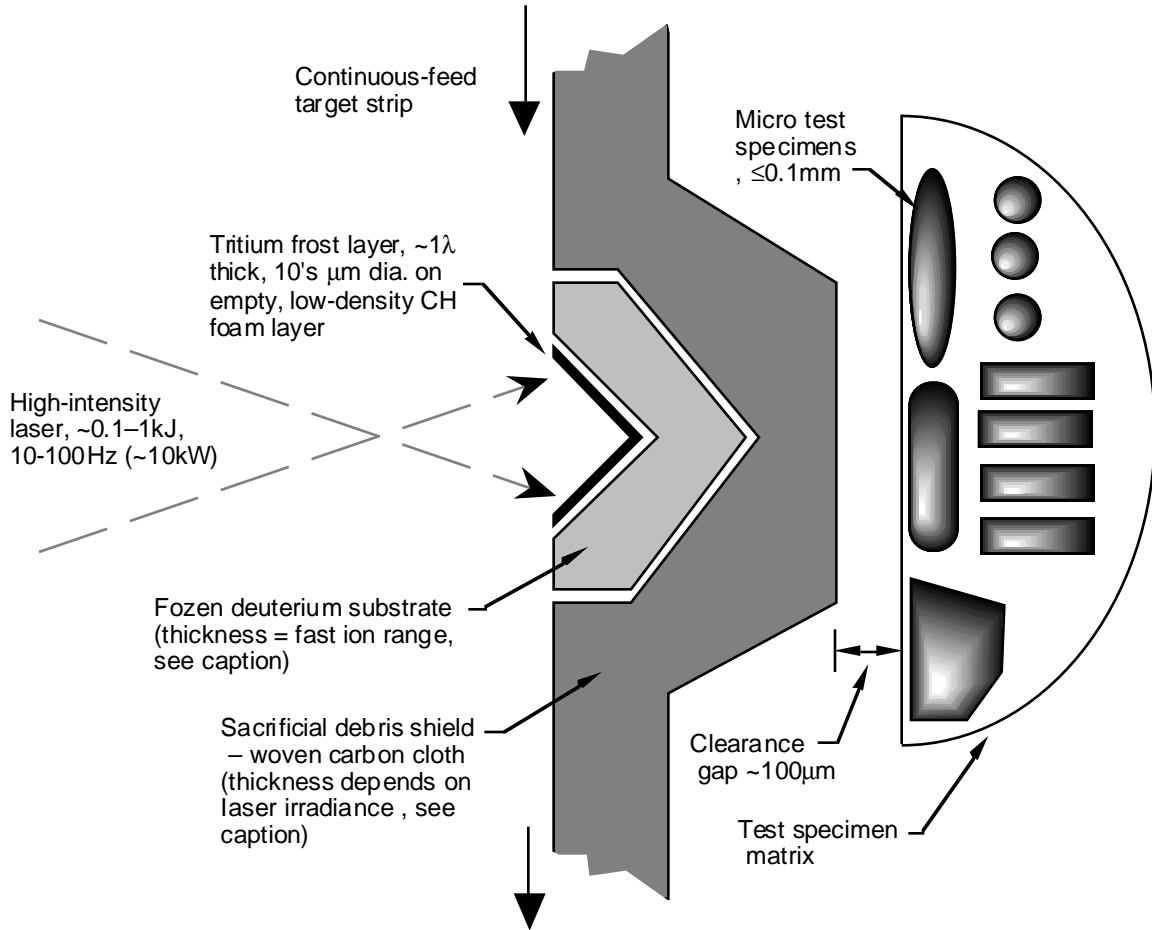


Fig. 2. Schematic of the target interaction region for Concept-1 (not to scale). The thicknesses of the deuterium substrate and debris shield are determined by the laser irradiance and resulting fast ion range and are described in Section 5 below. At high irradiances of  $I\lambda^2 > 10^{18}\text{W}\cdot\mu\text{m}^2/\text{cm}^2$ , the multilayer thin target system here may be replaceable by a thick, single region DT target.

Tritium ions slowing down in the deuterium substrate give rise to 14MeV fusion neutrons via  $\text{T}(\text{d},\text{n})^4\text{He}$  beam-target interactions. Concurrent ion and electron heating of the substrate decreases the ion stopping power resulting in longer ion ranges and significantly enhanced neutron production rates as the following analysis will demonstrate.

At lower laser intensities  $\leq 10^{17}\text{W}/\text{cm}^2$ , this process should be more efficient if the thin tritium layer is isolated from the deuterium substrate by a vacuum gap or a low density, insulating foam as shown Fig 1. In this way, the hot electrons are prevented from thermalizing in the substrate. Otherwise, a cold electron return current would occur, neutralizing the space-charge field accelerating the fast ions. At high intensities  $\geq 10^{18}\text{W}/\text{cm}^2$ , the single region,

thick target of Concept-2 may also yield an efficient hot ion current. The trends of this section are applicable to that target type also.

As was illustrated in Fig. 1 above, targets are mounted 1–10cm apart on a continuous plastic strip moving at about 0.1–10 m/s. We show below that laser energies of around 100–1000 J/pulse at rep-rates of ~10-100Hz (i.e. average powers of ~10kW) will be required to yield neutron fluxes  $\geq 10^{14}$  n cm<sup>-2</sup> s<sup>-1</sup> at material specimens mounted with stand-off distances of ~ millimeters from the target midpoint. A sacrificial shield of woven carbon cloth is sized to accommodate the laser blast and moves with the target strip to protect the material specimen from target debris.

An alternative option is to swap the tritium and deuterium regions so that the laser interacts in a thin deuterium layer and the resulting fast deuterium ions stream into a tritium substrate. While this produces higher neutron fluxes at lower ion energies because of the greater energy available in the center-of-mass for the DT cross section (see below), it will also result in significantly larger tritium inventories. In the scheme shown in Fig. 2, each target contains only about 4 $\mu$ Ci of tritium

To assess potential neutron yields and fluxes attainable with a candidate system, we introduce a 1-D slab model for laser interaction, ion slowing down and neutron production. We assume that the laser interaction with the thin, isolated tritium frost layer produces hot electrons of temperature  $T_{e,hot}$  which electrostatically couple to fast tritons yielding an initial mean fast ion energy  $\bar{E}_0$  incident on the deuterium substrate. As ions enter the substrate, they will begin to slow down transferring energy to the medium by ionization, excitation and drag. Concurrently, the substrate's temperature will begin to rise due to this ion deposition, supplemented by the fraction of laser-produced hot electrons not contributing to the space-charge-limited ion production. The total energy lost by an ion with local energy  $E_{ion}$  traversing a distance  $x$  in the substrate is

$$\Delta E(E_{ion}, T) = \int_0^x \frac{dE}{dx}(E_{ion}, T) dx \quad (6)$$

where  $\frac{dE}{dx}(E_{ion}, T)$  is the ion stopping power at substrate temperature  $T$ .

We assume the ion beam undergoes no angle scatter as it slows down (a good assumption until the end of range where neutron production is anyway negligible). Also, as we are always in the limit that the nuclear reaction cross section is small relative to the atomic slowing down cross sections, we can neglect ion removal from the beam. Therefore, for an ion beam of cross section area  $a_{ion}$  and flux  $\phi_{ion}$  ions cm<sup>-2</sup>s<sup>-1</sup>, the neutron production rate from a

slowing down element  $dx$  of volume  $A_{ion} \cdot dx$  at depth  $x$  into the substrate is  $n(x)\sigma(E_{ion}(x))\phi_{ion} a_{ion} dx$  where  $\sigma$  is the DT cross section at the local ion energy  $E_{ion}$ , depth  $x$  in the substrate and  $n$  is the local deuterium number density. Effecting a change of variable to the ion energy yields a total neutron yield in neutrons/second of

$$Y(\bar{E}_0, T) = nJ(E_l, I\lambda^2) \int_{\bar{E}_0}^0 \frac{\sigma(E_{ion})dE_{ion}}{dE / dx(E_{ion}, T)} \quad (7)$$

where  $\bar{E}_0$  is the initial mean kinetic energy of the ion beam entering the substrate and  $J(E_l, I\lambda^2) = a_{ion} \phi_{ion}$  is the fast ion current in ions/second, a function of the laser energy  $E_l$  and irradiance  $I\lambda^2$ . We also assume the deuterium density  $n$  is independent of depth in the target.

The resonance in the DT cross section,  $\hat{\sigma}$ , occurs at  $\sim 64$ keV in the center-of-mass [25]. In the lab frame, this translates to  $\sim 160$ keV for tritons incident on a deuterium target, or  $\sim 107$ keV for deuterons incident on a tritium target. However, because of the competition of atomic slowing-down, ion energies significantly greater than this peak are required to maximize the neutron yield in a thick beam-target system. The atomic cross sections due to drag and ionization and which contribute to the ion's stopping power,  $dE/dx$ , are significantly larger than the nuclear interaction cross section. Thus, in a cold target, the vast majority of ions slow down and stop in the target without producing a DT fusion reaction. Consequently, an ion starting out at high energy well above the peak in the fusion cross section has a greater chance of producing a fusion neutron before its energy is dragged down than an ion produced in the vicinity of the peak. Of interest here, a hot target with electron temperatures of 10's–100's eV has a significantly reduced  $dE/dx$ , thus enhancing the neutron yield for any ion birth energy. Of course, lower values of  $dE/dx$  imply higher neutron yields but also longer ion ranges and thus longer target-specimen displacements. Attention must be given, therefore, to both total yield and the neutron flux attainable at the specimen

Formalisms for ion energy deposition in matter at finite temperatures have been developed by Mehlhorn [26], where the stopping power can be generalized to:

$$\frac{dE}{dx}(E_{ion}, T) = \left(\frac{dE}{dx}\right)_{bound} + \left(\frac{dE}{dx}\right)_{nuc} + \left(\frac{dE}{dx}\right)_{free} + \left(\frac{dE}{dx}\right)_{ion} \quad (8)$$

and is a function of the average charge state  $\bar{Z}_1$  of the projectile ion of atomic number  $Z_1$  and the degree of ionization of the substrate,  $z_{eff}$  of atomic number  $Z_2$ . The first term in Eq. 8 accounts for energy loss due to ionization and excitation of bound electrons and is modeled by the Bethe equation [27] or, at

low energies, by the Linhard-Scharff-Schiott model [28]. Shell corrections are applied by Mehlhorn to both models. The second term represents elastic scattering between the ion and target nuclei of the substrate; it is only applicable at very low energies and particularly for large  $Z_1, Z_2$ . As the ion beam heats the substrate, the resulting ionization increases the number of free electrons which can participate in the slowing down process and reduces the number of bound electrons. The third and fourth terms in Eq. 4 account for the stopping power of these free electrons and resulting plasma ions, respectively. The ion term only becomes appreciable at high plasma temperatures where the ion thermal velocity is high. A medium with elevated plasma temperature can exhibit a significantly reduced total  $dE/dx$  over that of a cold target due to the substitution of the high stopping power of the bound electrons by smaller cross section of the free electrons. This has important consequences for neutron production efficiency.

Fig. 3 shows the application of Eq. 8 to our case where the stopping powers for tritons slowing on a solid-density deuterium substrate (solid line) are shown as a function of the ion energy with the plasma temperature of the substrate as a parameter. Deuterons slowing on a solid-density tritium substrate (dotted line) are shown for reference. Figure 4 shows the ion range resulting from our 1-D slab model. Note that at a target temperature of  $T \sim 1\text{keV}$ , the  $dE/dx$  is lowered by one to two orders of magnitude relative to a cold target ( $T=0$ ) with a commensurate increase in range.

Armed with this  $dE/dx$  formalism we can evaluate Eq. 7 to compute the neutron production efficiency for our laser-driven beam-target source. This is shown in Fig. 5 where the neutron yield per incident ion (i.e., with the fast ion current  $J$  in Eq. 7 set to unity) is plotted as a function of the initial mean kinetic energy  $\bar{E}_0$  of the ion beam incident on the substrate for a range of substrate temperatures. The DT fusion cross sections were taken from the latest evaluation by Bosch and Hale [25]. As these are thick target yields, the neutron production efficiencies increase monotonically with initial ion energy, and a knee in the yield curve is seen to occur around the peak in the DT cross section in the lab frame. Note the advantages of producing initial ion energies above  $\sim 200\text{keV}$  and realizing substrate temperatures in the vicinity of  $\sim 0.1\text{-}1\text{keV}$ .

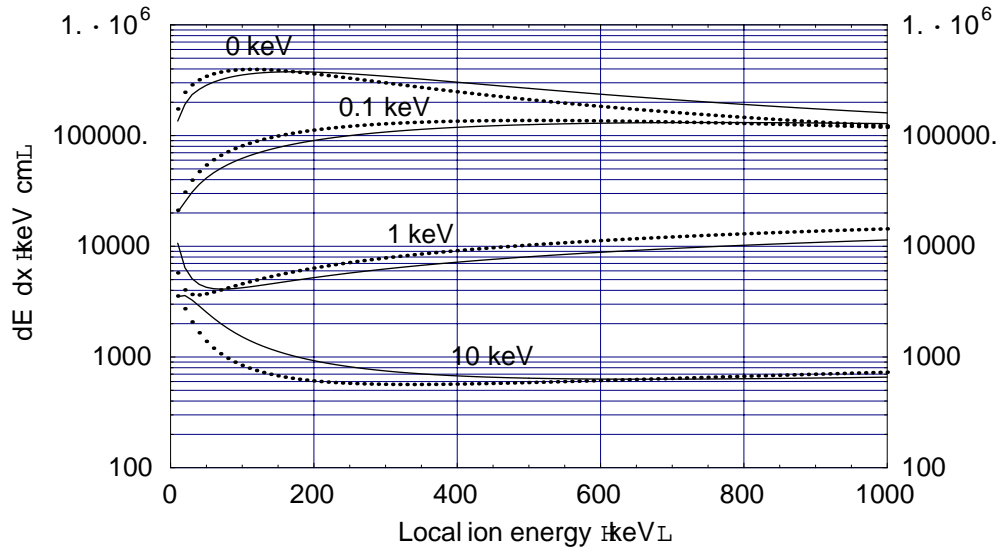


Fig. 3 Stopping power  $dE/dx$ , for tritons slowing down in a solid density deuterium substrate (solid line) and deuterons in a solid density tritium substrate (dotted line), as a function of the ion energy. The electron temperature of the substrate is shown as a parameter

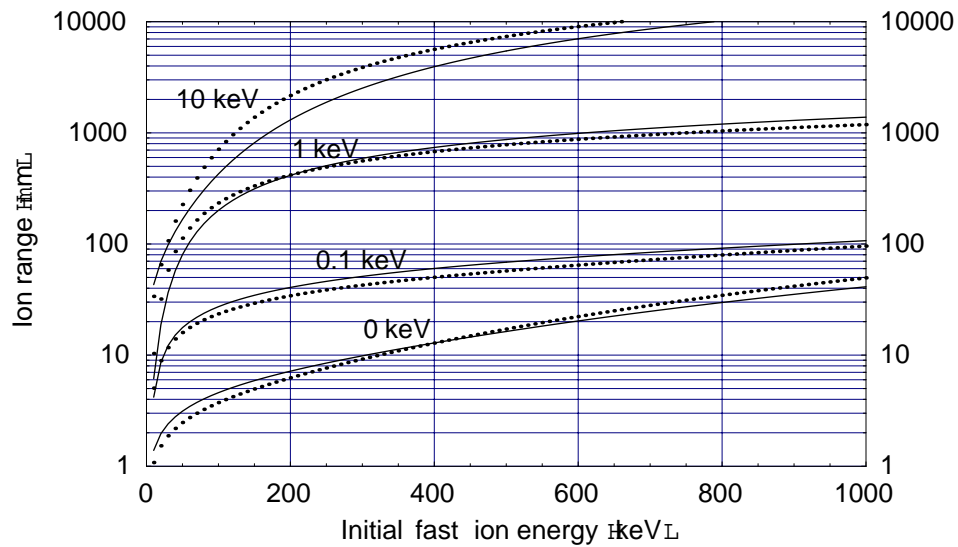


Fig. 4. Resulting ion ranges for the stopping powers shown in Fig. 3 above. The solid lines show the triton range in a solid density deuterium substrate while the dotted lines show the converse, and are plotted as a function of the initial ion energy. The electron temperature of the substrate is shown as a parameter

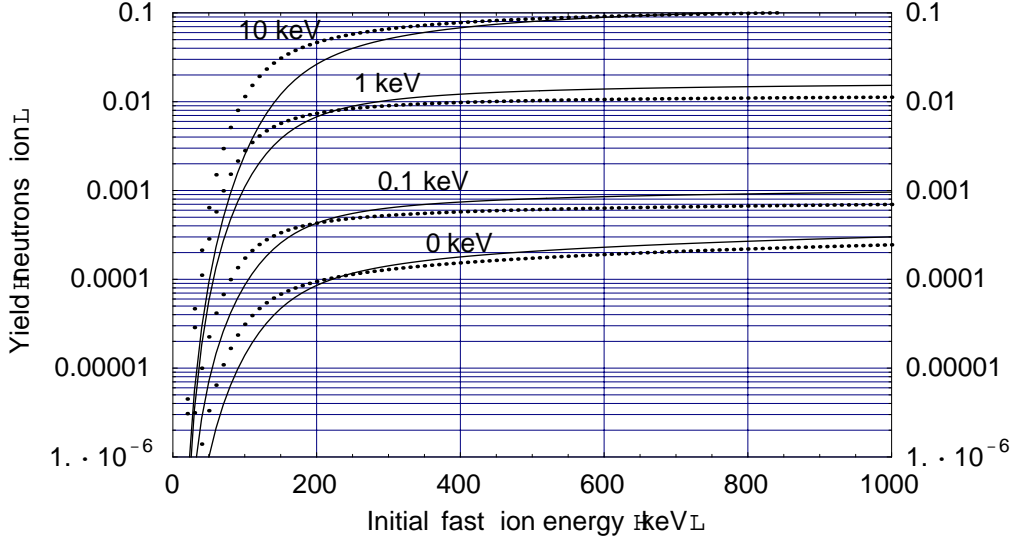


Fig. 5. 14MeV DT neutron production efficiency per incident ion for tritons interacting in a solid density deuterium substrate (solid lines) and deuterons interacting in a solid density tritium substrate (dotted lines) as a function of the initial ion energy. The electron temperature of the substrate is shown as a parameter

To compute neutron fluxes and absolute efficiencies, consider a laser, energy  $E_l$ , with pulse duration  $\tau$ , focal spot (FWHM) of  $d_l$ , wavelength  $\lambda$ , repetition rate  $r_l$  and irradiance  $I\lambda^2 = E_l\lambda^2 / (\pi d_l^2 \tau / 4)$  incident on the conical target shown in Fig. 2. Assuming an isotropic distribution of ions from the tritium frost layer, the fraction directed inwards towards the deuterium substrate is

$$f_{in} \approx 1 - \frac{0.5}{\sqrt{1 + (2A_{cone})^2}} \quad (9)$$

where  $A_{cone}$  is the cone aspect ratio, i.e. the ratio of the height to base diameter. In the limit of a flat surface (i.e.  $A_{cone} = 0$ ),  $f_{in} = 0.5$  as expected.

The absolute fast ion current into the substrate becomes

$$J(E_l, I\lambda^2) \approx \frac{E_l r_l (1 - \eta_{scatt}) \eta_{ion}(E_l, I\lambda^2) f_{in}}{\bar{E}_0(E_l, I\lambda^2)} \quad (10)$$

where  $\eta_{scatt}$  is the fraction of incident laser energy scattered from the front surface and  $\eta_{ion}$  is the conversion efficiency of absorbed laser light into fast ions of initial mean kinetic energy  $\bar{E}_0$

We obtain the fusion Q-value, i.e., the DT fusion energy output for a given incident laser energy input as:

$$Q_{DT} \approx \frac{Y(\bar{E}_0, T) \times 17.6 \text{ MeV}}{E_l r_l} \quad (11)$$

The 14MeV neutron flux at the front face of a material specimen is then

$$\phi_{DT} \approx \frac{Y(\bar{E}_0, T)}{4\pi L^2} \quad (12)$$

where L is taken as the distance from the midpoint of the ion slowing down range in the substrate – i.e., the midpoint of the neutron production region – to the front face of the specimen. This includes the carbon debris shield thickness  $t_d$  and clearance gaps,  $t_c$ , each side of the shield as:

$$L(\bar{E}_0, T) = 0.5R(\bar{E}_0, T) + t_d(E_l, \bar{E}_0, T) + 2t_c$$

where the ion slowing down range is  $R(\bar{E}_0, T) = \int_{\bar{E}_0}^0 \frac{dE_{ion}}{dE / dx(E_{ion}, T)}$

We use a spherical model to determine the thickness  $t_d$  of the sacrificial debris shield as  $t_d = 3x$ , where  $x$  is the real root of

$$\frac{E_l(1 - \eta_{scatt})}{4\pi x \left\{ R(\bar{E}_0, T) + t_c + \frac{x}{2} \right\}^2} = H_v \quad (13)$$

Here,  $H_v = 9.54 \times 10^4 \text{ J/cm}^3$  is the specific volumetric vaporization energy of woven carbon cloth was and obtained from the cohesive energy of carbon of 59.6MJ/kg [29] and a density of  $\sim 1.6 \text{ g/cm}^3$ . The factor of 3 ensures residual integrity of the shield over the minimum vaporization limit including a safety margin.

To parameterize the results for our concept, we take a laser, energy  $E_l = 100 \text{ J}$  with repetition rate  $r_l = 100 \text{ Hz}$  (average power = 10kW) and  $\lambda = 1 \mu\text{m}$ . We take clearance gaps of  $t_c \sim 100 \mu\text{m}$  each side of the debris shield. We assume a conical target of the type shown in Fig. 2 with an aspect ratio of  $A_{cone} = 2$ . Fig. 6 shows the fusion Q-value attainable (= DT fusion energy output divided by laser energy input) as a function of the initial fast ion energy  $\bar{E}_0$  with the substrate temperature  $T$  as a parameter and assumptions of  $\eta_{scatt} = 30\%$  and  $\eta_{ion} = 30\%$ ; that is, a net conversion efficiency of incident laser energy into fast

ions of 21%. Note, from Fig 6, that  $Q$  values tend to maximize for initial ion energies of  $\sim 150\text{-}250\text{keV}$  for deuterons incident on a tritium substrate and  $\sim 250\text{-}350\text{keV}$  for the converse. These trends are discussed further in Section 5 below where we perform self-consistent calculations of substrate temperatures.

Fig 7 shows the corresponding primary, uncollided 14MeV neutron flux at the front face of a specimen with source-specimen stand-off distances determined by Eq. 13 above. These are cycle-averaged fluxes in  $\text{n.cm}^{-2}\text{s}^{-1}$ , i.e. neutrons  $\text{cm}^{-2}$  pulse $^{-1}$  times the laser rep-rate. Note that if target temperature in the range  $\sim 100\text{-}1000\text{eV}$  could be sustained then neutron fluxes in the range  $10^{14}\text{-}10^{15}$   $\text{n.cm}^{-2}\text{s}^{-1}$  may be achievable. Note also that at high initial ion energies and high target temperatures, the flux at the specimen actually drops. This is due to the long slowing down range of such high energy ions in the high temperature substrate – see ion ranges in Fig. 4 above – which significantly increases the source-specimen distance  $L$  and decreases the

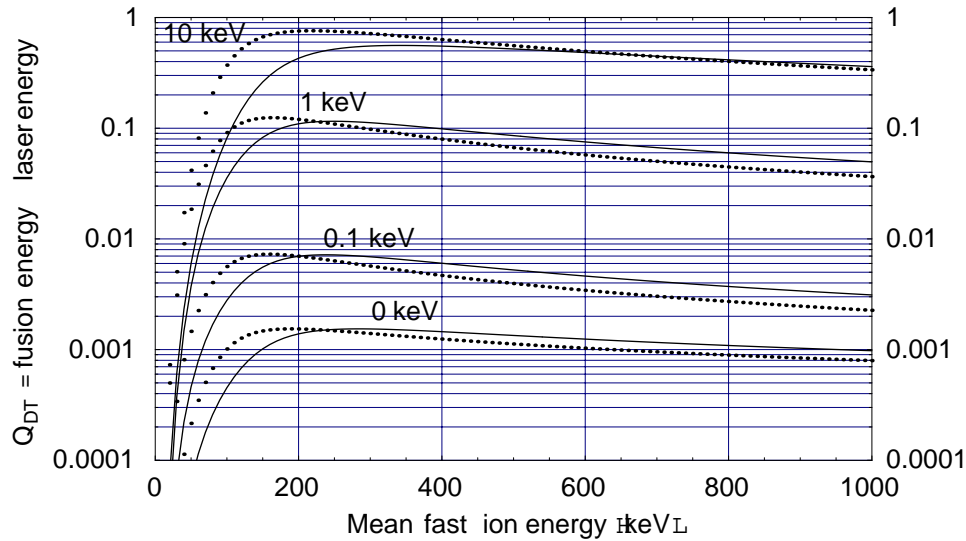


Fig. 6. DT fusion  $Q$  values (i.e. DT fusion energy output divided by laser energy input) as a function of the initial mean fast ion energy  $\bar{E}_0$  for a laser energy  $E_l = 100\text{J}$ , and assumptions of  $\eta_{\text{scatt}} = 30\%$  and  $\eta_{\text{ion}} = 30\%$ . The solid lines show tritons interacting in a solid density deuterium substrate while the dotted lines show deuterons interacting in a solid density tritium substrate. The electron temperature of the substrate is shown as a parameter

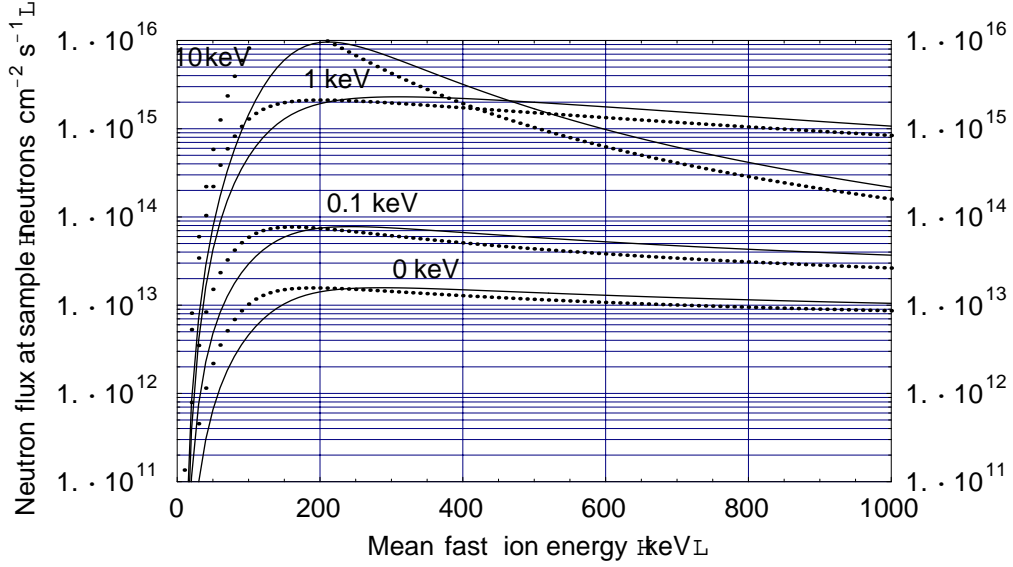


Fig. 7. 14MeV DT neutron flux at the front face of the specimen as a function of the initial mean fast ion energy  $\bar{E}_0$  for a laser energy  $E_l = 100\text{J}$  with repetition rate  $r_l = 100\text{Hz}$  (average power = 10kW), and assumptions of  $\eta_{\text{scatt}} = 30\%$  and  $\eta_{\text{ion}} = 30\%$ . The solid lines show tritons interacting in a solid density deuterium substrate while the dotted lines show deuterons interacting in a solid density tritium substrate. The electron temperature of the substrate is shown as a parameter. Target-sample standoff distances are a function of ion range and thus of  $\bar{E}_0$  and are discussed in the text

neutron flux as  $\sim 1/L^2$ . Consequently, optimum initial mean ion energies and target temperatures look to be in the range  $\sim 200\text{-}400\text{keV}$  and  $\sim 100\text{-}1000\text{eV}$ , respectively. We note below that these fluxes depend on the feasibility of closed-coupled target-specimen standoffs of  $\sim 0.1\text{-}0.2\text{cm}$  and running clearances of  $\sim 100\mu\text{m}$ .

In Section 5, below we work an approximately self-consistent case for fast ion production, substrate temperature and resulting neutron production as a function of laser conditions.

#### 4. Exploding Pusher Neutron Source (Concept-3)

Here, we consider targets comprising DT micro-spheres of radius several 10's of  $\mu\text{m}$  in radius encased in a thin glass shell of a few  $\mu\text{m}$  thickness. Hot electrons generated by the high intensity laser absorbing on the outside of the shell penetrate the entire target and heat the glass shell rapidly to  $>2\text{keV}$ , exploding it with several gigabar pressure and driving an inward

shock of  $\geq 5 \times 10^7$  cm/s. The center-of-mass of the shell or ‘pusher’ is almost stationary as it explodes both inward and outward. Since the DT fuel is preheated, it is on a high isentrope, so the fuel radius converges only a factor of a few [30]. The convergent shock heats the DT core to  $\sim 10$ keV.

Such electron-conduction-driven ‘exploding pusher’ targets were the most common types of targets utilized in the early stages of the ICF program and were the first type to produce thermonuclear neutrons [30]. They can more easily achieve higher implosion velocities than conventional hot-spot targets and, due to their low convergences, are more tolerant of asymmetries in the drive. However, they do not scale to high gain because all the target mass is on a high isentrope which precludes high compression

We employ the LASNEX simulation code [31] to find optimal targets with the following fixed assumptions: A laser energy of 1 kJ, and wavelength of 1.06  $\mu\text{m}$  is symmetrically illuminating the glass, DT filled micro-spheres. A fixed fraction of 20% of that energy is assumed to be absorbed, and the energy is distributed into a ‘hot electron’ thermal distribution, whose temperature  $T_H$  is given by the formula

$$T_H = 30.0 (I\lambda^2)^{0.4} \text{ keV} \quad (14)$$

This formula is in reasonable agreement with data from short pulse, high intensity laser plasma interaction experiments and with Eqs. 1 and 4 from Section 2. Here the laser intensity  $I$  is in units of  $10^{17}\text{W}/\text{cm}^2$  and the wavelength  $\lambda$  is in units of 1.06  $\mu\text{m}$  light. The hot electrons then transport their energy throughout the target (chiefly heating the dense glass shell) as well as driving the expansion of the outer part of the target.

In the optimization search, we varied the pulse length of the laser, the radius of the shell, the thickness of the shell, and the fill density of the DT fuel. The quantity  $T_H$  varies as we change the pulse length or shell radius, since at fixed energy, the intensity  $I$  varies inversely with the pulse length and  $R^2$ . In general the optimization procedure converged rapidly, by following the scaling arguments presented in Rosen and Nuckolls [32]

Yields in excess of  $10^{12}$  neutrons were produced by several combinations of parameters: For example a 60 $\mu\text{m}$ -radius, 3 $\mu\text{m}$ -thick shell illuminated by a 15ps FWHM Gaussian pulse and filled with 0.025 g/cm<sup>3</sup> DT gas, converged a factor of 3 from initial fuel-pusher radius to minimum fuel-pusher radius. As another example, a 45 $\mu\text{m}$ -radius, 4.5 $\mu\text{m}$ -thick shell illuminated by a 15ps FWHM Gaussian pulse and filled with 0.05 g/cm<sup>3</sup> DT gas also exceeded  $10^{12}$  neutrons. In both examples peak ion temperatures

exceeded 10 keV. Thus, a 10Hz driver would supply  $\sim 10^{14}$  n.cm<sup>-2</sup>s<sup>-1</sup> at a sample 1mm away from these targets.

All of these results were purely from one-dimensional simulations. The effect of two- and three-dimensional asymmetries on capsule performance need to be addressed in future studies. Tradeoffs between the performance of one and two-sided illumination versus the requisite expense of two-sided illumination driver schemes cannot be answered without such analyses.

In the absence of definitive 2-D and 3-D models, further 1-D studies have been performed for targets that could be illuminated by a petawatt class facility. Here, we hold fixed a 400 J laser source. An optimization study, otherwise identical to that described above, found target parameters that yielded  $10^{11}$  neutrons, more than enough for detection. For example a 30 $\mu$ m-radius, 3 $\mu$ m-thick shell illuminated by a 7.5ps FWHM Gaussian pulse and filled with 0.05 g/cm<sup>3</sup> DT gas achieved such a yield, with a convergence factor slightly larger than 3. Clearly, experiments may be within reach that can assess the predictions and, in particular, explore the cost tradeoffs of illumination asymmetry performance.

As an aside, we also note that LASNEX simulations have also been performed by Callahan-Miller [20] on heavy-ion-driven, exploding pusher targets. She obtained yields of  $\sim 5 \times 10^{13}$  neutrons/pulse from the deposition of 5 kJ of heavy-ions in  $\sim 35$ ps into a 10 $\mu$ m gold shell surrounding a 35  $\mu$ m-radius cryogenic DT core. This represented a fusion gain of  $Q \sim 0.3\%$

## 5. Candidate Design Points for Concept-1

In this section, we extend the 1-D slab model from Section 3 above to obtain an approximately self-consistent case for fast ion production, substrate temperature and resulting neutron production as a function of the laser intensity for the target design of Concept-1.

We assume that we are operating in the medium irradiance regime (i.e.,  $I \lambda^2 \leq 10^{18}$  W- $\mu$ m<sup>2</sup>/cm<sup>2</sup>) with a target design of the form shown in Fig. 2. above. We also assume that the laser energy is initially absorbed by the electrons via collisional absorption followed by subsequent transfer to fast ions which are responsible for heating the target substrate material. Thus, determination of the ion  $dE/dx$  and resulting range in the substrate requires the determination of the coupled, time-dependent substrate temperature,  $T$ , according to

$$\frac{d}{dt}(3nkT) \approx \frac{E_i \eta_{ion} (1 - \eta_{scatt})}{V_{subst}(T, \bar{E}_0) \tau_{eff}(T, \bar{E}_0)} - \frac{3nkT}{\tau_E(T, \bar{E}_0)} - P_{rad}(T) \quad (15)$$

The first term on the rhs is the power deposited per unit volume in the substrate due to fast ions. Here,  $V_{subst}(T, \bar{E}_0)$  is the heated substrate volume and is a function of substrate temperature  $T$  (one-fluid model) and the initial mean fast ion kinetic energy  $\bar{E}_0$  through the ion slowing-down range. The effective time constant for ion heating of the substrate is taken as  $\tau_{eff}(T, \bar{E}_0) \approx \sqrt{\tau^2 + \tau_{ion}^2}$ , and is determined by the longer of the laser pulse length,  $\tau$ , or the time for ions to be accelerated across the sheath and slow down in the substrate,  $\tau_{ion}$ . The second term on the rhs of Eq. 15 is the rate of thermal energy loss. As each side of the substrate is a vacuum boundary, we neglect electron heat conduction and take  $\tau_E(T, \bar{E}_0) \sim R(T, \bar{E}_0) / c_s(T)$  where  $R(T, \bar{E}_0)$  is the substrate thickness set equal to the ion slowing-down range and  $c_s(T)$  is the sound speed for disassembly. The third term is radiation loss via Bremsstrahlung which scales as  $\sim T^{1/2}$

Table 2 shows the results of applying Eq. 15 to the target design of Fig. 2 for the following laser conditions: Energy/pulse  $E_i = 100\text{J}$ , repetition rate  $r_i = 100\text{Hz}$  (average power =  $10\text{kW}$ ),  $\lambda = 1\mu\text{m}$ , a focal spot size (FWHM) of  $d_f = 20\mu\text{m}$ , and where the laser irradiance is varied from  $I\lambda^2 = 10^{15}$  to  $10^{19}\text{W}\cdot\mu\text{m}^2/\text{cm}^2$  by adjusting the pulse length  $\tau$  from  $3.18 \times 10^{-8}\text{s}$  to  $3.18 \times 10^{-12}\text{s}$ , respectively. At each irradiance, we apply Gitomer's empirical scaling from Eq. 1 to obtain the initial hot electron temperature of the tritium frost layer and then deduce the mean energy of the expelled fast ions  $\bar{E}_0$  by the sheath potential through which they are accelerated as expressed by Eq. 2. As the literature does not yet reveal consistent scalings for the efficiency of fast ion production versus  $I\lambda^2$ , we assume  $\eta_{scatt} = 30\%$  and  $\eta_{ion} = 30\%$  as in section 3. From Eq 15, we then solve for the resulting target temperature and optimum substrate thickness, where the latter is determined by the ion slowing-down range  $R(T, \bar{E}_0)$ . Finally, from the formalisms of Eq. 7 through 13, we compute the resulting neutron yield, the required carbon debris shield thickness, the standoff distance from the target to the material test specimen, and the neutron flux at the front face of the latter.

We see from Table 2, that the mean fast ion energies range from  $\sim 25\text{keV}$  at  $I\lambda^2 = 10^{15}\text{W}\cdot\mu\text{m}^2/\text{cm}^2$  to  $\sim 1.5\text{MeV}$  at  $I\lambda^2 = 10^{19}\text{W}\cdot\mu\text{m}^2/\text{cm}^2$ . For the upper three decades of  $I\lambda^2$ , the substrate temperature is around a keV and is only a weak function of irradiance because the increased heating rate is balanced by a longer ion range and thus a larger volume for power deposition. Below  $\sim 10^{16}\text{W}\cdot\mu\text{m}^2/\text{cm}^2$ , the substrate temperature falls rapidly.

Table 2. Target parameters as a function of laser irradiance,  $I\lambda^2$ , for laser specifications of 100J/pulse, 100Hz rep rate, a focal spot diameter (FWHM) of 20 $\mu$ m, and a pulse duration determined by the irradiance requirement below .

	Laser Irradiance $I\lambda^2$ (W- $\mu$ m <sup>2</sup> /cm <sup>2</sup> )				
	$10^{15}$	$10^{16}$	$10^{17}$	$10^{18}$	$10^{19}$
Laser power (W)	$3.14 \times 10^9$	$3.14 \times 10^{10}$	$3.14 \times 10^{11}$	$3.14 \times 10^{12}$	$3.14 \times 10^{13}$
Required pulse duration <sup>a</sup> (s)	$3.18 \times 10^{-8}$	$3.18 \times 10^{-9}$	$3.18 \times 10^{-10}$	$3.18 \times 10^{-11}$	$3.18 \times 10^{-12}$
Hot electron temperature of T <sub>2</sub> frost layer (keV)	7.43	20.7	57.5	160	445
Mean fast ion energy $\bar{E}_0$ (keV)	25.2	70.0	195	542	1510
Fast ion range in D <sub>2</sub> substrate (cm) (= optimum substrate thickness)	0.00133	0.0102	0.0636	0.170	0.307
Mean substrate temperature $T$ (keV)	0.144	0.651	1.81	1.80	1.58
Neutron yield (s <sup>-1</sup> )	$1.71 \times 10^{11}$	$3.21 \times 10^{13}$	$6.69 \times 10^{14}$	$5.44 \times 10^{14}$	$2.05 \times 10^{14}$
Fusion Q value	$4.8 \times 10^{-5}$	0.0091	0.19	0.15	0.058
Required carbon debris shield thickness (cm)	0.145	0.130	0.0638	0.0183	0.00653
Target–specimen stand-off distance (cm) <sup>b</sup>	0.165	0.155	0.116	0.123	0.179
14MeV neutron flux at sample (cm <sup>-2</sup> s <sup>-1</sup> ) <sup>c</sup>	$4.98 \times 10^{11}$	$1.06 \times 10^{14}$	$3.99 \times 10^{15}$	$2.85 \times 10^{15}$	$5.09 \times 10^{14}$

a. Determined by required laser irradiance ( $I\lambda^2$ ) at fixed energy and focal spot size.      b. Center of target substrate to front face of specimen (see Section 3).  
c. Measured at the front face of specimen; mid-specimen fluxes would be little different due to their small size (~100 $\mu$ m).

Also from Table 2. we note an optimum in the fusion Q and the neutron flux at the specimen around  $I\lambda^2 \sim 10^{17}\text{--}10^{18}\text{W}\cdot\mu\text{m}^2/\text{cm}^2$ , a result of three factors: (a) increasing mean fast ion energy with increasing  $I\lambda^2$  means less total fast ions for the fixed laser energy of 100J/pulse and fixed  $\eta_{ion}$ , (b) higher mean fast ion energies give diminishing returns relative to the peak of the DT cross section at 160keV, (c) higher mean fast ion energies have longer ion ranges in the substrate thus requiring greater substrate thicknesses and greater standoff distances to the sample. Thus, given this model, irradiances of  $I\lambda^2 \sim 10^{17}$  appear to be optimum to maximize the 14MeV neutron flux at the front face of the specimen at  $\sim\text{few}\times 10^{15}\text{ cm}^{-2}\text{s}^{-1}$  for this target type. Caveats include:

- Our thin-target, electron-space-charged-limited model for fast ion acceleration may not be applicable at  $I\lambda^2 \geq 10^{18}$  where the hot electrons become relativistic and direct fast ion production becomes efficient (see Section 2 above). An option here perhaps is to switch to a single region DT target as in Concept-2.
- We assumed a constant fast ion production efficiency of  $\eta_{ion} \sim 0.3$  [6-7, 13, 17, 22-24] although, in reality, this is a complex function of  $I\lambda^2$  and target conditions. Quantitative experiments are required to determine predictive behavior.
- The neutron fluxes in Table 2 are computed at the front face of the specimens. Due to the small size of the samples ( $\sim 100\mu\text{m}$ ), the mid-specimen fluxes would only fall by  $\sim 10\%$ . However, the numbers in Table 2 also assume the attainment of closed-coupled specimens with target-specimen standoff distances of  $\sim 0.1\text{--}0.2\text{cm}$ . Should larger clearances of, say,  $0.5\text{cm}$ , be required in a fully practical, system, these fluxes will be reduced by a factor of  $\sim 10$  to a  $\sim\text{few}\times 10^{14}\text{ cm}^{-2}\text{s}^{-1}$

The capital cost of a full irradiation facility based on the results of Table 2 for a 10kW-average-power laser system, might be in the range  $\sim \$150\text{--}200\text{M}$ . This crude estimate is based on a laser and target facilities cost of  $\sim \$50\text{--}100\text{M}$  obtained by scaling with power from the present Mercury, diode-pumped, solid-state experimental facility at LLNL [34]. Also, we assume  $\sim \$100\text{M}$  for conventional facilities including shielded experimental areas and hot cells per the conceptual design of the IFMIF International Fusion Materials Irradiation Facility [10]. For approximately  $\$50\text{M}$  less, we might consider a 1kW-average-power system and reductions in neutron flux by an order of magnitude or so.

## 6. Materials Research and Computational Modeling Requirements

Capabilities for multi-scale, predictive modeling of radiation-induced microstructure and mechanical property changes in irradiated materials are reaching a high degree of sophistication. Physically-based modeling and simulation tools can be coupled across all relevant length and time scales [35]. Of course, such models require stringent validation in order to become fully viable predictive tools. The 14 MeV neutron source concepts proposed here offer the potential to irradiate materials at different temperatures, fluxes and pulse rates. When coupled with advanced, post-irradiation assay techniques, these results would play a crucial role in the development and validation of such multiscale modeling tools which can then be applied to predict the extrapolated behavior of full-size, engineering-scale materials

At the shortest time scale, molecular dynamics (MD) simulations on ASCI-class massively-parallel computers can describe the form of the primary damage state [36-38], i.e., the number and state of clustering of the produced defects as a function of recoil energy. To link the time scales, kinetic Monte Carlo (KMC) methods are used to determine how the produced defects are able to escape their nascent cascade and migrate through the lattice to produce microstructural and micro-chemical changes [36, 39-43]. This linked MD/KMC simulations can be carried out at doses and dose rates identical to those used in a given set of irradiation experiments. Their output is the spatial and temporal distribution of defects, impurity atoms, voids, impurity precipitates, and sink (dislocation) microstructure.

To predict how these microstructure features alter the mechanical properties of the irradiated material, new three-dimensional dislocation dynamics simulation tools can be employed [44-48]. Such simulations provide a complete description of the plastic behavior of a single grain of material and of the microstructure development under an applied load, including the locking and immobilization of dislocation by irradiation-induced loops and precipitates. Moreover, the simulations provide a prediction of the stress-strain curve for a given starting microstructure and thus a prediction of the yield stress and the strain hardening exponents as a function of irradiation dose. Finally, the constitutive relations obtained from these fundamental studies can then be used to provide predictive strength models for polycrystalline materials for use in continuum computer code simulations including full 3-D finite element codes

These modeling studies would be validated with the experimentally testing of post-irradiated specimens using techniques such as micro-mechanical testing, transmission electron microscopy, and synchrotron-based X-ray diffraction [35]. The small dimensions of the irradiated specimens (~100-1000 $\mu\text{m}$ ) envisaged for use here do not present any fundamental difficulty regarding experimental characterization of the irradiated volumes. While the

small volume cannot generate direct data on the behavior of actual engineering-scale materials, the combination of the irradiation, testing and multiscale modeling programs can provide extrapolated data to predict actual engineering structure performance.

In inertial confinement fusion (ICF) systems, the response of structural materials to the pulsed nature of neutron irradiation can be very different when compared to steady irradiation. It is shown in Refs. 48 and 49 that significant theoretical and experimentally verifiable differences exist between pulsed and steady state fusion systems. Under some conditions, materials response at the same dose and temperature is enhanced, while the response is reduced under other conditions, as compared with steady irradiation. Fission reactor irradiation by itself may not represent anticipated materials response under intense irradiation pulsing. Major differences are demonstrated for irradiation swelling [51, 52], irradiation creep [53, 54], point defect production [55], and irradiation hardening [52].

Under intense pulsed irradiation, the temporal rate of damage production is significantly increased, leading to well-known rate effects on the response of materials. Clustering of point defects is enhanced, and point defect recombination is also increased. This is a direct result of such reactions being of a non-linear nature, similar to second-order chemical reactions. In the mean time, if the off time between radiation pulses is long, and the temperature is high, some annealing of radiation damage would occur in an accelerated fashion. The influence of these processes on radiation hardening, creep, and swelling is well documented in references [48-52].

The proposed micro neutron source can be a unique experimental facility to explore these basic aspects of pulsed irradiation for applications in ICF fusion systems, if the pulse frequency is adjusted to be  $\sim 10$  Hz. Here, materials response is expected to be quite different from steady-irradiation. The main reason being that the vacancy mean lifetime can be shorter than 0.1 second at elevated temperatures, thus enhancing annealing kinetics of the microstructure. On the other hand, if the pulse frequency is greater than  $\sim 50$  Hz, it is generally expected that the response of the material will be equivalent to that under steady fusion irradiation. Thus, by adjusting the pulse repetition rate, the facility could be tailored to give information on both ICF and magnetically-confined fusion systems that no other facility will be able to deliver at this time.

## **7. Recommendations for Further R&D**

- Quantify the interaction of fast-pulse, high intensity lasers with low-Z matter, particularly the mechanisms for high efficiency, fast ion production. Determine the dependence of fast ion energy, spectra and

production efficiency on the laser energy and irradiance. In particular, determine the irradiance regime that may allow us to dispense with the multilayer target of Concept-1 above and move to efficient direct fast ion production in the simpler, single-layer target of Concept-2.

- Perform representative experiments with candidate targets to project neutron yields and fusion gains that may be attainable with affordable laser energies of  $\sim 10\text{J}$  to  $1\text{kJ}$  and rep-rates of  $\sim 10\text{-}100\text{Hz}$ . Characterize the requirements for associated debris shields that will ensure specimen integrity during irradiation periods. (Note that the initial experimental determination of attainable neutron yields with optimized targets can be performed with single-shot laser facilities and can be low cost).
- Couple state-of-the-art PIC modeling with beam-target neutron production in hot substrates to: (a) complement the experimental program described above, (b) resolve physics uncertainties in the transition from low intensities to higher intensities, especially the effects of relativistic hole boring, electron transport with co-generated high magnetic fields and direct laser-field coupling to ions, and (c) perform fully self-consistent 2-D calculations for neutron yield under concurrent substrate heating.
- For the exploding pusher target concept, perform two- and three-dimensional modeling studies to determine the effect of asymmetries on capsule performance and, thereby, elucidate the tradeoffs of multi-sided illumination.
- Perform engineering designs of practical laser-target systems for the attainment of uncollided  $14\text{MeV}$  fluxes in the range  $\sim 10^{14}\text{-}10^{15}\text{ n.cm}^{-2}\text{s}^{-1}$  and fluences equivalent to  $\sim 100\text{dpa}$ . In particular, determine required standoff (couple with experimental results above), protection and data-acquisition needs for close-coupled micro-materials specimens
- Develop 100-mm-scale sample holders for stress and temperature control of fiber/wire specimens during irradiation. Develop advanced, post-irradiation assay techniques and multiscale predictive modeling tools which, when coupled to such irradiated micro-samples, can be applied to predict the extrapolated behavior of full-size, engineering-scale materials

## Acknowledgments

The authors take pleasure in acknowledging informative discussions with:

M. Key, G. Guethlein, E. M. Campbell, P. Springer, S. Wilkes, P. Rambo, T. C. Sangster, H. Powell, C. Bibeau and K. Estabrook of Lawrence Livermore National Laboratory, A. Rowcliffe and S. Zinkle of Oak Ridge National Laboratory, and T. Mehlhorn of Sandia National Laboratory.

This work was performed under the auspices of the U.S. Department of Energy by Lawrence Livermore National Laboratory under contract number W-7405-Eng-48

## References

- [1] C. C. Baker, et al., *Technical Planning Activity – Final Report*, Chapter 5, Argonne National Laboratory, ANL/FPP-87-1 (1987). see also, M. A. Abdou, et al., *Nucl Fusion* **27**, 619 (1987)
- [2] S. Cierjacks, et al., *Nucl. Sci Eng.* **106**, 99 (1990)
- [3] M. D. Perry, G. Mourou, *Science* **264**, 917 (1994)
- [4] P. Gibbon, E. Forster, *Plasma Phys Control. Fusion* **38**, 769 (1996)
- [5] T. Ditmire, et al., *Nature* **386**, 54 (1997)
- [6] T. Ditmire, et al., *Phys. Rev. Lett.* **78**, 3121 (1997)
- [7] R. W. Petzoldt, R. W. Moir, *Fusion Technology* **30**, 73 (1996)
- [8] D. G. Doran et al., *Evaluation Committee on the Los Alamos Spallation Radiation Effects Facility: Final Report*, PNL-SA-18584, Battelle Pacific Northwest Laboratory (1990). See also, S. D. Harkness et al., *Fusion Energy Advisory Committee Panel Report on the Fusion Materials Research Program*, Westinghouse Electric Company (1998)
- [9] D. W. Heikkinen, C. M. Logan, J. C. Davis, *Nucl. Sci. Eng.*, **106**, 228 (1990)
- [10] T. E. Shannon et al, "Conceptual Design of the International Fusion Materials Irradiation facility (IFMIF)", paper S30-033 in *Eighth Internat. Conf. on Fusion Reactor Materials*. To be published in *J. Nucl. Mater.* (1998)
- [11] W. L. Kruer, *The Physics of Laser Plasma Interactions*, (Addison-Wesley, 1988)
- [12] D. W. Forslund, *Phys. Rev. Lett.* **48**, 1614 (1982)

- [13] S. J. Gitomer et al., *Phys Fluids*, **29**, 2679 (1986)
- [14] R. A. Gross, *Fusion Energy*, p132 (J. Wiley, 1984)
- [15] W. L. Kruer and K. G. Estabrook *Phys. Fluids* **20**, 1688 (1977). See also, K. G. Estabrook and W. L. Kruer *Phys. Rev. Lett.* **40**, 42 (1978), K. R. Manes et al., *J. Opt. Soc. Amer.* **67**, 717 (1977), W. L. Kruer, *The Physics of Laser Plasma Interactions*, (Addison-Wesley, 1988), p159-160
- [16] A. P. Fews et al., *Phys. Rev. Lett.* **73**, 1801 (1994)
- [17] S. C. Wilks et al., *Phys. Rev. Lett.* **69**, 1383 (1992)
- [18] D. D. Meyerhofer et al., *Phys Fluids B* **5**, 2584 (1993)
- [19] G. Guethlein, Lawrence Livermore National Laboratory, Livermore, CA, personal communication (1998)
- [20] G. Pretzler et al., *Phys. Rev. E* **58**, 1165 (1998)
- [21] P. A. Norres et al., *Plasma Phys Control. Fusion* **40**, 175 (1998)
- [22] J. Denavit, *Phys. Rev. Lett.* **69**, 3052 (1992)
- [23] W. S. Lawson et al., *Phys Plasmas* **4**, 788 (1997)
- [24] M. D. Perry, Lawrence Livermore National Laboratory, Livermore, CA, personal communication (1998)
- [25] H. S. Bosch and G. M. Hale, *Nucl. Fusion* **32**, 611 (1992)
- [26] T. A. Mehlhorn, *J. Appl. Phys.* **52** 6522 (1981)
- [27] See for example, J. D. Jackson, *Classical Electrodynamics*, p618ff (J. Wiley, 1975)
- [28] J. Linhard, et al., *Mat. Phys. Medd.* **33**, 14 (1963)
- [29] Chemical Rubber Company, *Handbook of Chemistry and Physics*, 55th ed., (CRC Press, 1974)
- [30] J. Lindl, *Inertial Confinement Fusion*, (AIP Press, Springer-Verlag, 1998)
- [31] G. B. Zimmerman, W. L. Kruer, *Comments Plasma Phys.* **2**, 51 (1975)

- [32] M. D. Rosen, J. H. Nuckolls, *Phys. Fluids* **22**, 1393 (1979)
- [33] D. Callahan-Miller, Lawrence Livermore National Laboratory, Livermore, CA, personal communication (1998)
- [34] C. Marshall, et al. "Next Generation Laser for Inertial Confinement Fusion", p318 in *Optical Society of America Trends in Optics and Photonics*, Vol **19** Advanced Solid State Lasers, W. Bosenberg and M. Fejer, Eds., (Optical Society of America 1998)
- [35] D. Lassila, et al., "Dislocation Dynamics at the Microscale", *FY99 Strategic Initiative Proposal to the Laboratory Directed Research and Development Program*, Lawrence Livermore National Laboratory (1998).
- [36] T. Diaz de la Rubia, *Ann. Rev. Mater. Sci.* **26**, 613 (1996)
- [37] R. S. Averback, T. Diaz de la Rubia, *Solid State Physics* **51**, 281 (1998)
- [38] D. J. Bacon, et al, *J. Nucl. Mater.* **251**, 1 (1997)
- [39] H. L. Heinisch, *Nucl. Instr. Methods B* **102**, 47 (1995)
- [40] H. L. Heinisch, B. N. Singh, *J. Nucl. Mater.* **251**, 77 (1997)
- [41] N. Soneda, T. Diaz de la Rubia, *Philos. Mag. A*, in press (1998)
- [42] T. Diaz de la Rubia et al., *J. Nucl. Mater.* **251**, 13 (1997)
- [43] N. M Ghoniem, *J. Nucl. Mater.*, **179** 99-104 (1991).
- [44] L. P. Kubin, G. Canova, *Scripta Metall.* **27**, 957 (1993)
- [45] L. P. Kubin, *Treatise in Materials Science and Technology*, R.W. Cahnet al, eds, (VCH: Weinum FRG, 1993)
- [46] M. Rhee et al, *Model. Sim. in Mater. Sci. and Eng.* in press (1998)
- [47] H. Huang et al., "Stability of Dislocation Short-range Reactions in BCC Crystals," submitted to *J. Eng. Mat. & Tech* (1998)
- [48] N. M. Ghoniem "Curved parametric segments for the stress field of 3-d dislocation loops" Submitted to *J. Eng. Mat. & Tech.* (1998)

- [49] N. M. Ghoniem, G. L. Kulcinski, *Nucl. Technol./Fusion*, **2**,165 (1982)
- [50] E. P. Simonen, N. M. Ghoniem, and N. H. Packan, *J. Nucl. Mater.* **122&123**, 391 (1984)
- [51] N. M. Ghoniem, G. L. Kulcinski, *J. Nucl. Mater.* **85&86**, 547 (1979).
- [52] N. M. Ghoniem, *J. Nucl. Mater.* **89**, 359 (1980)
- [53] H. Gurol, N. M. Ghoniem, and W. G. Wolfer, *J. Nucl. Mater.* **99**, 1 (1981).
- [54] H. Gurol, N. M. Ghoniem, and W. G. Wolfer, *J. Nucl. Mater.* **103-104**, 251 (1981).
- [55] M. E. Sawan, G. L. Kulcinski, and N. M. Ghoniem, *J. Nucl. Mater.* **103-104**, 109-113 (1981)